**Supplementary Data**

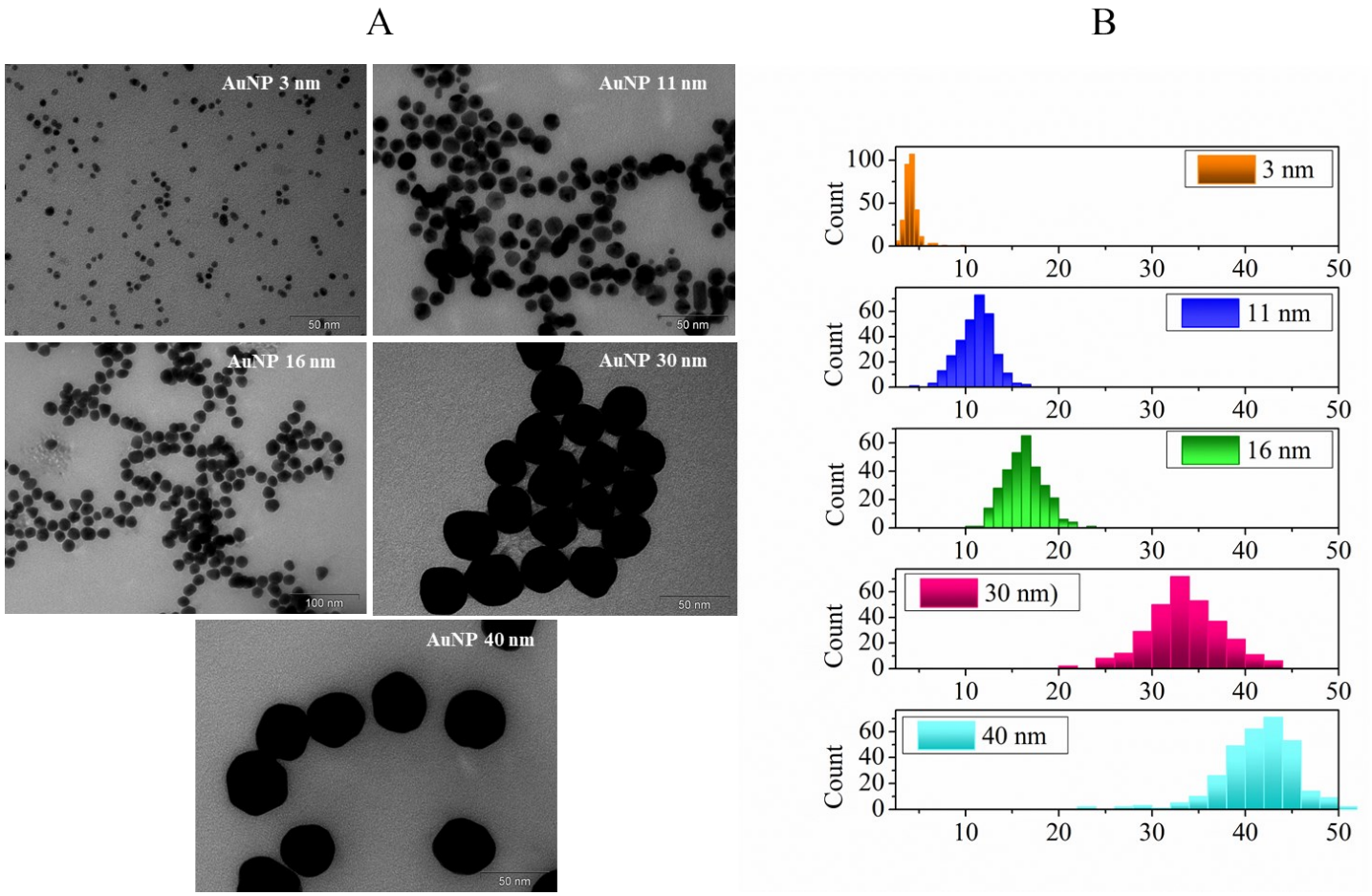


**Figure S1.** Citrate-coated AuNP used in this study. (A) TEM imaging of AuNP and, (B) core size distribution from TEM imaging.

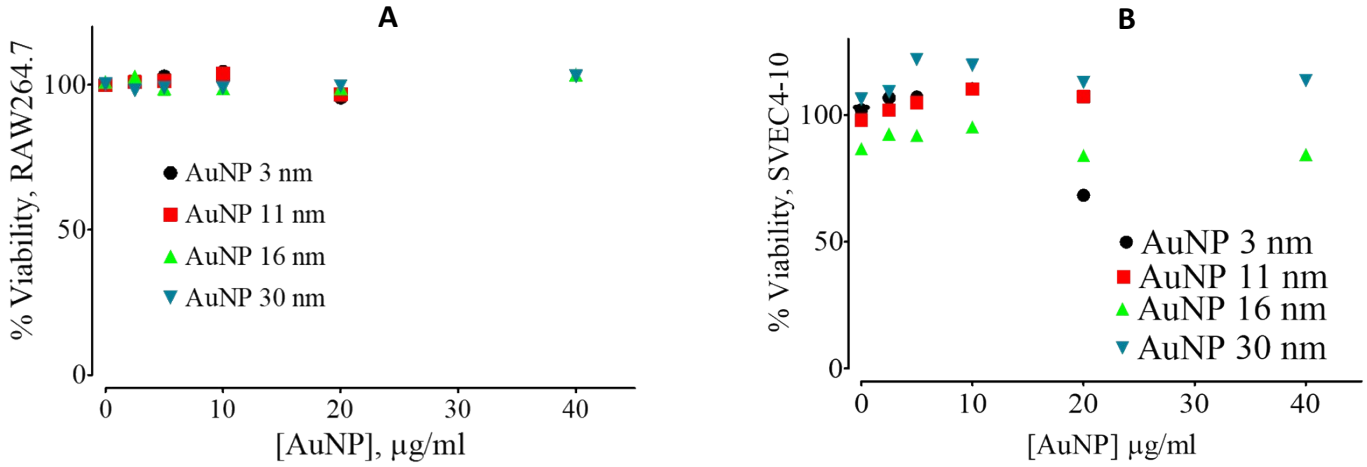


**Figure S2.** Viability assessed through Alamar blue metabolic activity test for macrophages RAW264.7 (A) and endothelial cells SVEC4-10 (B) incubated with AuNPs of different diameters (3, 11, 16 and 30 nm) for 24 hours at different concentrations.

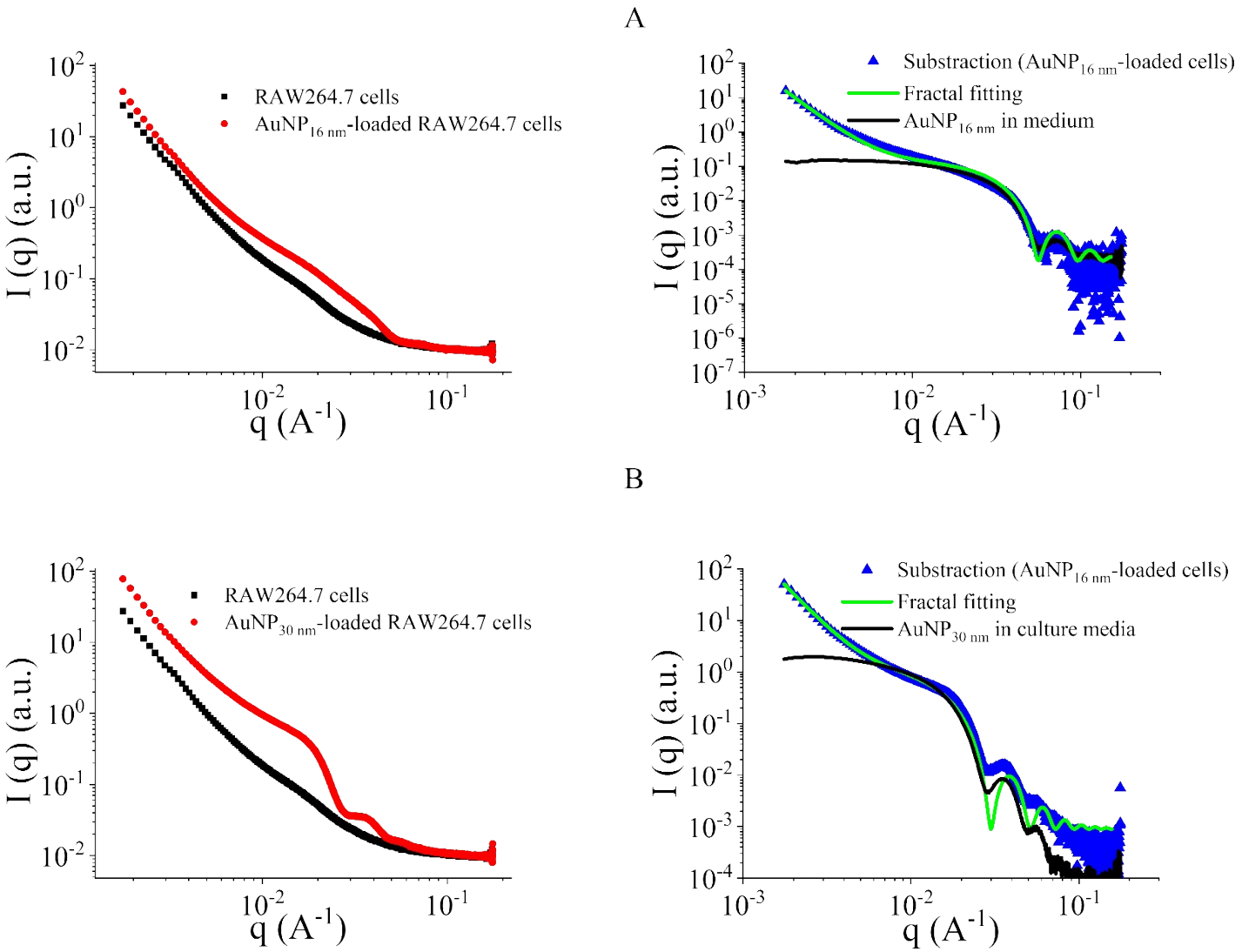


**Figure S3.** Fractal re-arrangement of endocytosed AuNP in RAW264.7 cells according to SAXS analysis for 16 nm (A) and 30 nm (B). Left: dark curves correspond to sole RAW264.7 cell scattered x-ray intensity and red curves to AuNP-loaded cell signals. Right: blue curves correspond to the AuNP-loaded cell signal after subtraction of the unloaded cell signal, green curve to a 3-D analysis by fractal model fitting, and black curves to 10 μg/ml AuNP in culture media (DMEM+10% FBS).

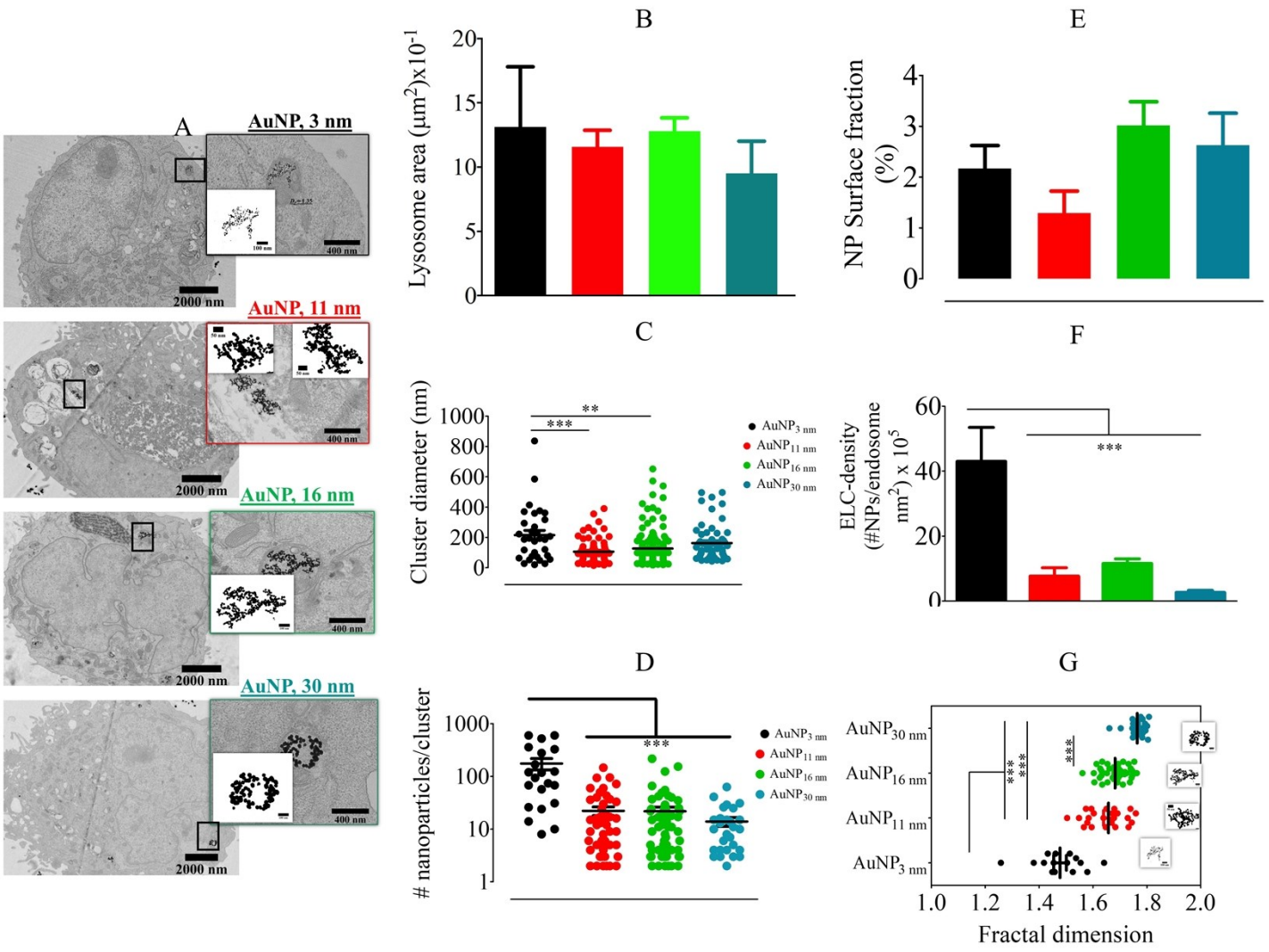


**Figure S4.** Internalization of gold nanoparticles by murine endothelial cell line, SVEC4-10 (A) TEM imaging of AuNP-loaded SVEC4-10 cells; *insets* emphasize intracellular AuNP clusters. (B) Area of NPs-containing endolysosomes as determined by TEM imaging. (C) Intracellular cluster diameter. (D) The number of nanoparticles per intracellular cluster. (E) Surface fraction covered by intracellular AuNP. (F) Endolysosome-limited cluster density (ELC density) of AuNPs. (G) 2-D fractal dimensions of intracellular AuNP clusters; *inset*s represent exemplary binary fractals. Significance, $^{*}p<0.05$, $^{**}p<0.01$, $^{***}p<0.001$, one-way ANOVA test, with post-test Bonferroni for comparison of all pair of columns.

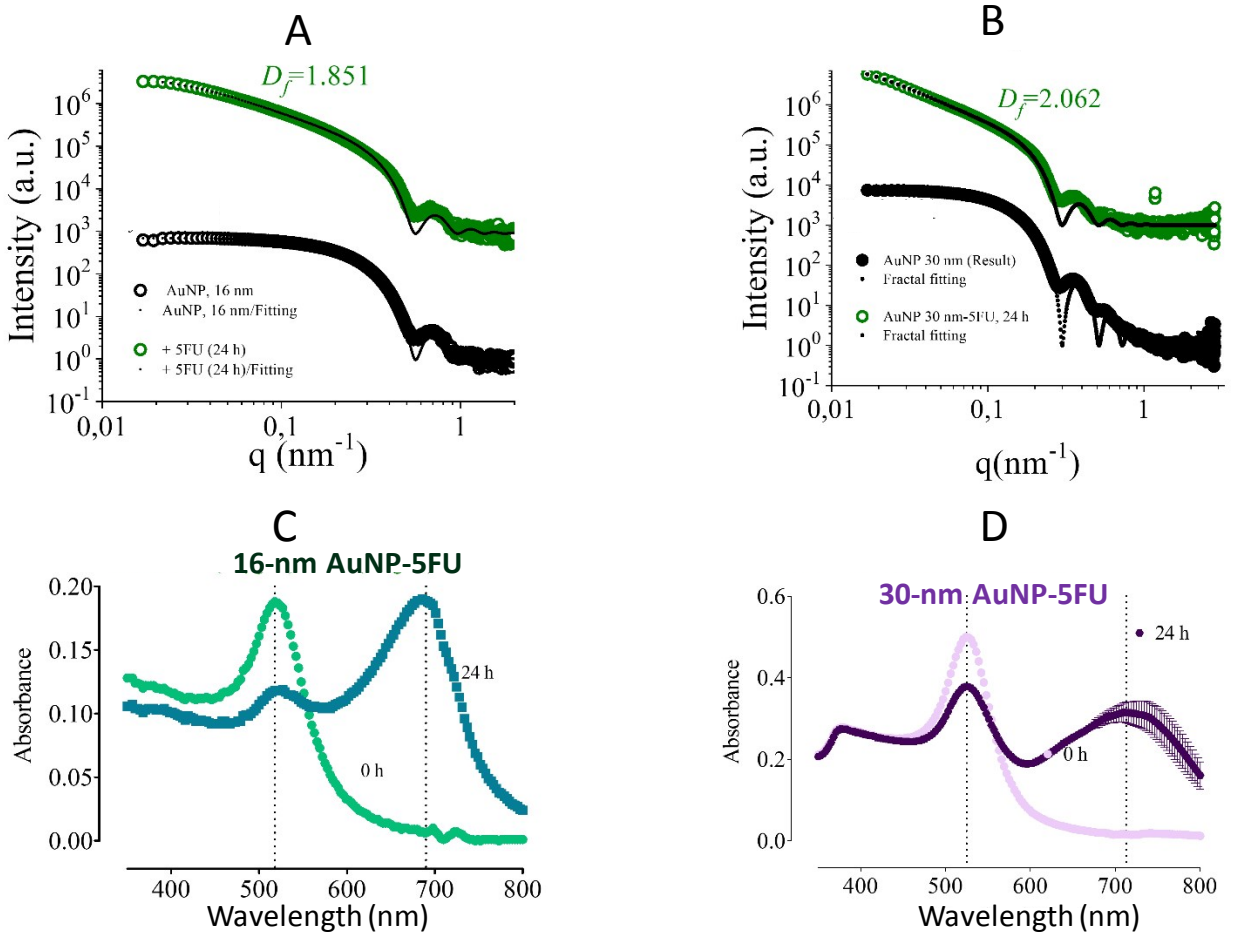


**Figure S5.** Characterization of 16 nm- and 30 nm AuNP-5FU complexes 24 hours after mixing. (A-B) Small-angle X-ray scattering (SAXS) profiles obtained at t=24 hours after mixing of 16 nm-AuNPs (A) and 30 nm-AuNPs (B) with 5-FU (green curves) in comparison with the SAXS profile of AuNPs alone (black curves). The continuous black lines correspond to the best adjustment of the mass fractal model and fixed particle characteristics (R = 8 nm, PD 0.21) and (R= 15 nm, PD 0.22). The mass fractal dimension of 16 nm-AuNPs and 30 nm-AuNPs are found to be, respectively, 1.85 and 2.06. The curves have been shifted by decades for clarity. (C-D) UV-vis-NIR spectra of 16-nm AuNPs-5FU (C) and 30 nm AuNPs-5FU (D) complexes at t=0 and at t=24 hours after mixing indicating the rise of a second LSPR band around 700 nm.

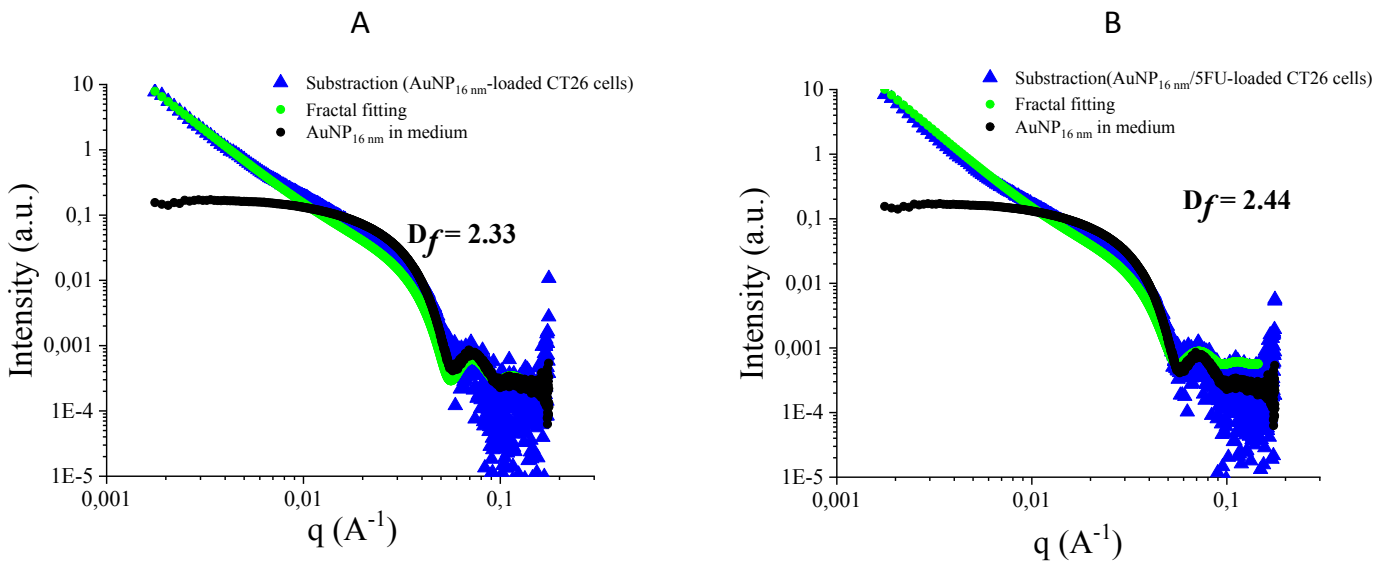


**Figure S6.** Fractal re-arrangement of endocytosed 16 nm-AuNP (A) and pre-aggregated 16 nm AuNPs-5FU complexes (B) in CT26 colon carcinoma cells according to SAXS analysis. Blue curves correspond to the AuNP-loaded cell signal after subtraction of the unloaded cell signal, green curve to a 3-D analysis by fractal model fitting, and black curves to 10 µg/ml 16 nm AuNP in culture media (DMEM+10% FBS). Mass fractal dimension $D_f$ is of 2.33 for 16nm-AuNPs loaded in CT26 cells, and 2.44 for pre-aggregated 16 nm AuNPs-5FU complexes loaded in CT26 cells.

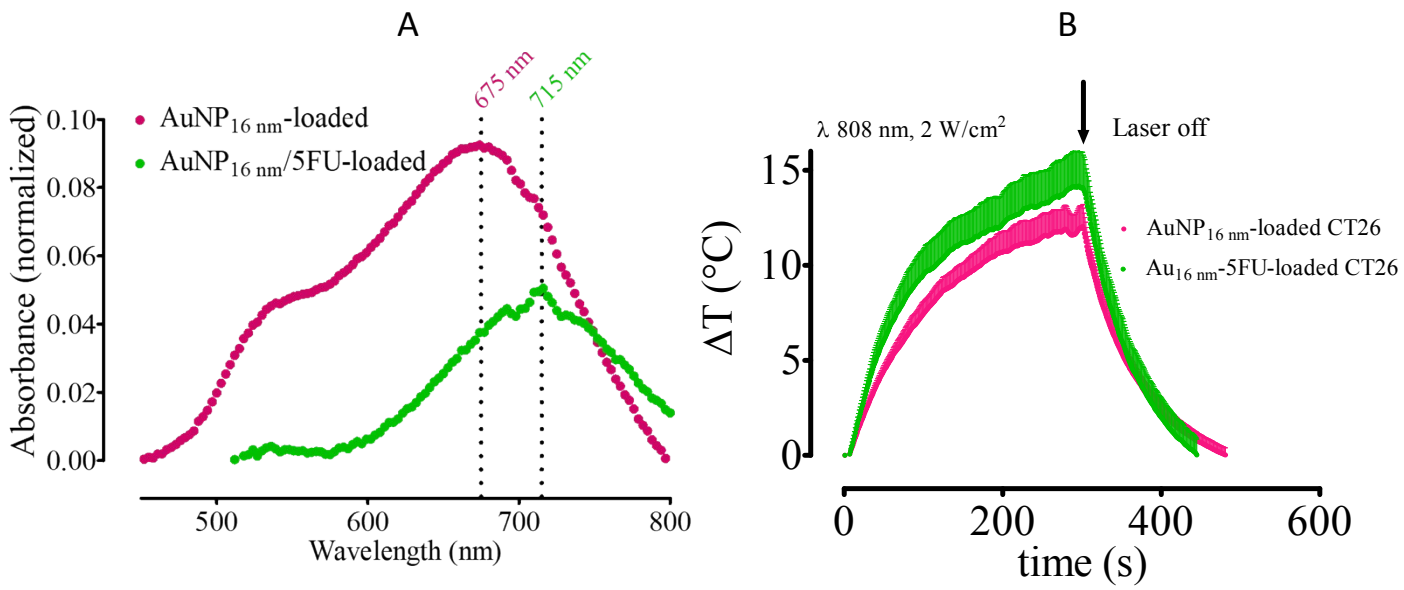


**Figure S7**. Optical and photothermal properties of 16 nm-AuNPs and 16 nm-AuNP-5FU complexes internalized in CT26 colon carcinoma cells. (A) **The** UV-vis-NIR spectrum of CT26 cells after internalization of 16 nm-AuNPs and 16 nm-AuNP-5FU complexes (10 μg/ml, 24 h). Highlighted wavelengths stand for the maximum secondary LSPR. (B) Temperature curves measured in a pellet of CT26 cells after internalization of 16 nm-AuNPs and 16 nm-AuNP-5FU complexes (10 μg/ml, 24 h) under irradiation with an 808 nm-laser for 5 minutes at 2 W.cm².

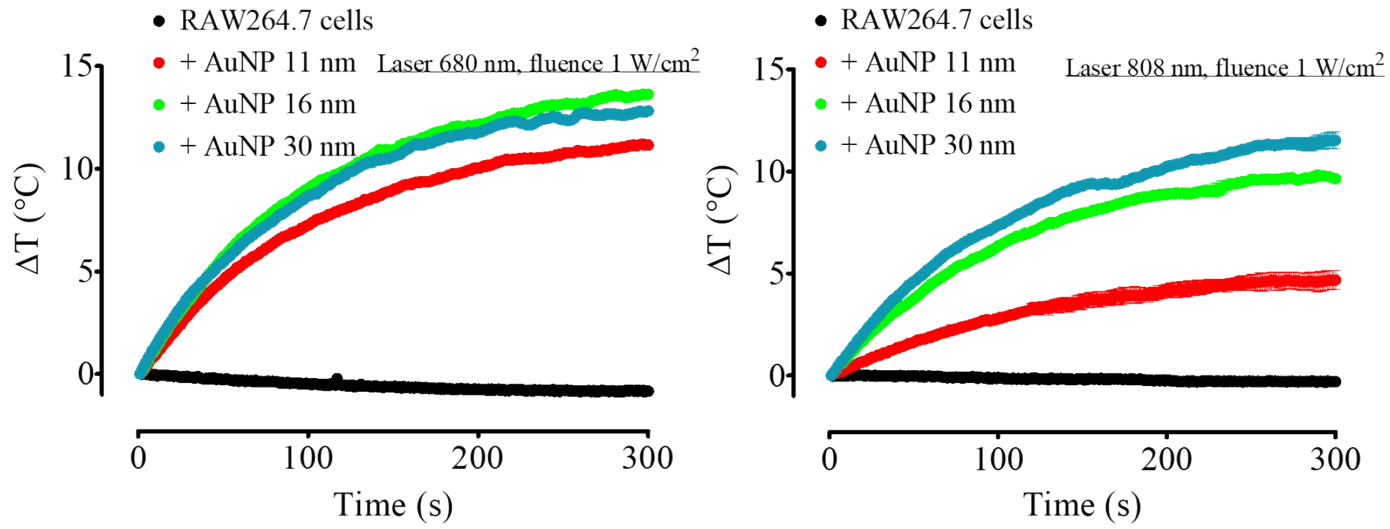


**Figure S8.** Heating capacity of RAW264.7 cells after 24 h of incubation with 10 μg/ml AuNP and upon irradiation with a 680 nm- or an 808 nm- laser at 1 W/cm². A similar tendency can be observed when compared to the application of a 3.57 W/cm² fluence.

. **Table S1**: table of the average values used for statistical analysis

| Sample name | Cell type | NP_diam | 5-FU complex | Lyso_area | Clust_diam | Nb_NPs _clust | Surf_frac | ELC_dens | 2D_FD | Plasm_ wl | Plasm_ int | DeltaT_ 680 | DeltaT_ 808 |
|---|---|---|---|---|---|---|---|---|---|---|---|---|---|
| RAW_3nm | RAW | 3 | No | 0.53 | 169.0 | 239.9 | 82.8 | 38.2 | 1.53 | 613.4 | 15.9 | 28.6 | 13.5 |
| RAW_11nm | RAW | 11 | No | 1.58 | 149.7 | 47.2 | 20.2 | 6.0 | 1.69 | 659.9 | 26.7 | 34.3 | 14.2 |
| RAW_16nm | RAW | 16 | No | 1.20 | 239.0 | 67.8 | 19.4 | 3.7 | 1.69 | 690.5 | 34.2 | 35.2 | 17.4 |
| RAW_30nm | RAW | 30 | No | 0.80 | 249.8 | 32.0 | 6.6 | 6.7 | 1.77 | 776.2 | 54.2 | 33.2 | 25.7 |
| SVEC_3nm | SVEC | 3 | No | 0.41 | 215.0 | 175.8 | 43.0 | 25.6 | 1.48 | 608.8 | 12.6 | 29.9 | 9.1 |
| SVEC_11nm | SVEC | 11 | No | 0.29 | 105.8 | 22.2 | 7.7 | 6.4 | 1.66 | 637.6 | 16.7 | 25.6 | 9.3 |
| SVEC_16nm | SVEC | 16 | No | 0.19 | 126.8 | 21.8 | 11.6 | 4.1 | 1.68 | 668.0 | 18.4 | 23.0 | 12.1 |
| SVEC_30nm | SVEC | 30 | No | 0.52 | 162.8 | 13.9 | 2.7 | 1.1 | 1.76 | 712.2 | 22.8 | 21.8 | 14.2 |
| CT26_16nm | CT26 | 16 | No | 1.08 | 93.7 | 9.7 | 9.6 | 3.4 | 1.58 | 651.5 | 14.4 | 22.0 | 17.8 |
| CT26_30nm | CT26 | 30 | No | 0.61 | 210.6 | 14.1 | 6.0 | 1.0 | 1.76 | 713.0 | 30.2 | 22.1 | 26.6 |
| CT26_16nm_5FU | CT26 | 16 | Yes | 1.56 | 728.2 | 129.7 | 13.1 | 2.6 | 1.77 | | | | 19.8 |
| CT26_30nm_5FU | CT26 | 30 | Yes | 3.12 | 858.5 | 165.0 | 10.5 | 1.8 | 1.82 | | | | 12.7 |

**Table S2**: correlation values between the descriptive variables and the three first principal components of the PCA

| | **PC1** | **PC2** | **PC3** |
|---|---|---|---|
| Lyso_area | 0.297 | 0.814 | -0.350 |
| Clust_diam | 0.263 | 0.845 | -0.360 |
| Nb_NPs_clust | -0.656 | 0.704 | 0.080 |
| Surf_frac | -0.854 | 0.255 | 0.365 |
| ELC_dens | -0.870 | 0.141 | 0.406 |
| 2D_FD | 0.884 | 0.271 | -0.186 |
| Plasm_wl | 0.898 | -0.034 | 0.362 |
| Plasm_int | 0.731 | 0.199 | 0.632 |
| DeltaT_680 | -0.043 | 0.529 | 0.599 |
| DeltaT_808 | 0.680 | 0.007 | 0.471 |